

Establishing Direct Phenomenological Connections between Fluid and Structure by the Koopman-Linearly- Time-Invariant Decomposition

Cruz Y. Li^{1,2} (李雨桐), Zengshun Chen^{1*} (陈增顺), Tim K.T. Tse^{3**} (谢锦添), Asiri Umenga Weerasuriya⁴, Xuelin Zhang⁵ (张雪琳), Yunfei Fu⁶ (付云飞), Xisheng Lin⁷ (蔺习升)

¹ *Department of Civil Engineering, Chongqing University, Chongqing, China*

^{2,3,4,6,7} *Department of Civil and Environmental Engineering, The Hong Kong University of Science and Technology, Hong Kong SAR, China*

⁵ *School of Atmospheric Sciences, Sun Yat-sen University, Zhuhai, China.*

¹ yliht@connect.ust.hk; ORCID 0000-0002-9527-4674

² zchenba@connect.ust.hk; ORCID 0000-0001-5916-1165

³ timkttse@ust.hk; ORCID 0000-0002-9678-1037

⁴ asiriuw@connect.ust.hk; ORCID 0000-0001-8543-5449

⁵ zhangxlin25@mail.sysu.edu.cn; ORCID 0000-0003-3941-4596

⁶ yfuar@connect.ust.hk; ORCID 0000-0003-4225-081X

⁷ xlinbl@connect.ust.hk; ORCID 0000-0002-1644-8796

* Co-first author with equal contribution.

** Corresponding author

All correspondence is directed to Dr. Tim K.T. Tse.

The main text (excluding figures) fits within four pages in single-space, meeting the length requirement of Physics of Fluids Letters.

Abstract

In this work, we introduce a novel data-driven formulation, the Koopman-Linearly-Time-Invariant (Koopman-LTI) decomposition, for analyzing Fluid-Structure Interactions (FSI). An implementation of the Koopman-LTI on a subcritical free-shear flow over a prism at $Re=22,000$ corroborated the construction of a configuration-wise universal approximation of nonlinear fluid-structure dynamics with stellar accuracy. It also successfully decomposed the entwined morphologies of raw numerical measurement into a linear superposition of distinct frequency-based constituents. Most importantly, even with random and anisotropic turbulence, the Koopman-LTI yielded identical modes for fluid motions and wall pressures, permitting direct connections of fluid and structural phenomena with phenomenological visualization.

Introduction

Despite centuries of scientific exploration, Fluid-Structure Interactions (FSI) remain an enigma of knowledge and a quandary of engineering applications. From the authors' perspective, the difficulty of FSI is trifold. First, a fluid system is infinite-dimensional, in which every fluid particle pertains to a unique motion. The spatiotemporal content of the motion is also governed by complex nonlinear dynamics [1]. Second, measurement of turbulence derives from highly volatile and entwined morphologies, meaning the user-recorded field or structural response is, in reality, an amalgam of thousands of fluid phenomena acting together [2]. Therefore, the isolation of these mechanisms is critical, but often a task of Hercules. Third, the interactive mechanisms of FSI are sophisticated, nonlinear, and deeply esoteric [3]. To date, we still struggle to establish lucid links between the fluid and structural behaviors.

Without a solution for the Navier-Stokes (NS) equations, the analytical path to tackling FSI is drenched with thorns and obstacles. Nevertheless, recent advancements in computer science shed new light by luminating the data-driven route. A collection of pioneering work on data-driven FSI has been produced in fluid mechanics [4], [5], biomedical engineering [6], [7], civil engineering [8], [9], *etc.* To this end, the data-driven Koopman analysis emerges as a brilliant method to overcome the aforementioned difficulties [10]–[13].

Theoretically, by imposing a mapping Koopman operator A to connect two data sequences $U_2 = AU_1$, one performs a global linearization to a nonlinear system. The acquisition of A via the similarity approach \tilde{A} , as proposed by Tu et al. [14] and Schmid [15] for the Dynamic Mode Decomposition (DMD), permits reduced-order modeling (ROM) through Singular-Value

Decomposition (SVD)-based formulations. Then, $\tilde{\mathbf{A}}$ is quintessentially a data-driven, implicit representation of the Navier-Stokes. It is also increasingly more accurate with dimensionality, and transforms into the exact Navier-Stokes with infinite-dimensionality. More importantly, a theoretical possibility exists for $\tilde{\mathbf{A}}$ to reduce into a linearly time-invariant (LTI) system. If so, applying the Eigen-Ritz decomposition to $\tilde{\mathbf{A}}$ effectively reconstructs the input data as a superposition of a consistent set of linear constituents:

$$U_{LTI}(\mathbf{x}, t) = \sum_{i=1}^n \alpha_i \phi_i e^{\omega_i t} = \boldsymbol{\alpha} \boldsymbol{\Phi} e^{\boldsymbol{\Omega} t} \quad (1)$$

where $U_{LTI}(\mathbf{x}, t)$ denotes the reconstructed data at location \mathbf{x} and time t , $\boldsymbol{\alpha}$ contains the leading coefficients, $\boldsymbol{\Phi}$ contains the eigenfunctions (*i.e.*, DMD modes or Z-space poles), and $\boldsymbol{\Omega}$ contains the eigenvalues (*i.e.*, modal frequencies). **Fig. 1** illustrates the conceptual process of the Koopman-LTI decomposition. We also refer the readers to [16] for the full mathematic formation of DMD, which is used to obtain the LTI systems.

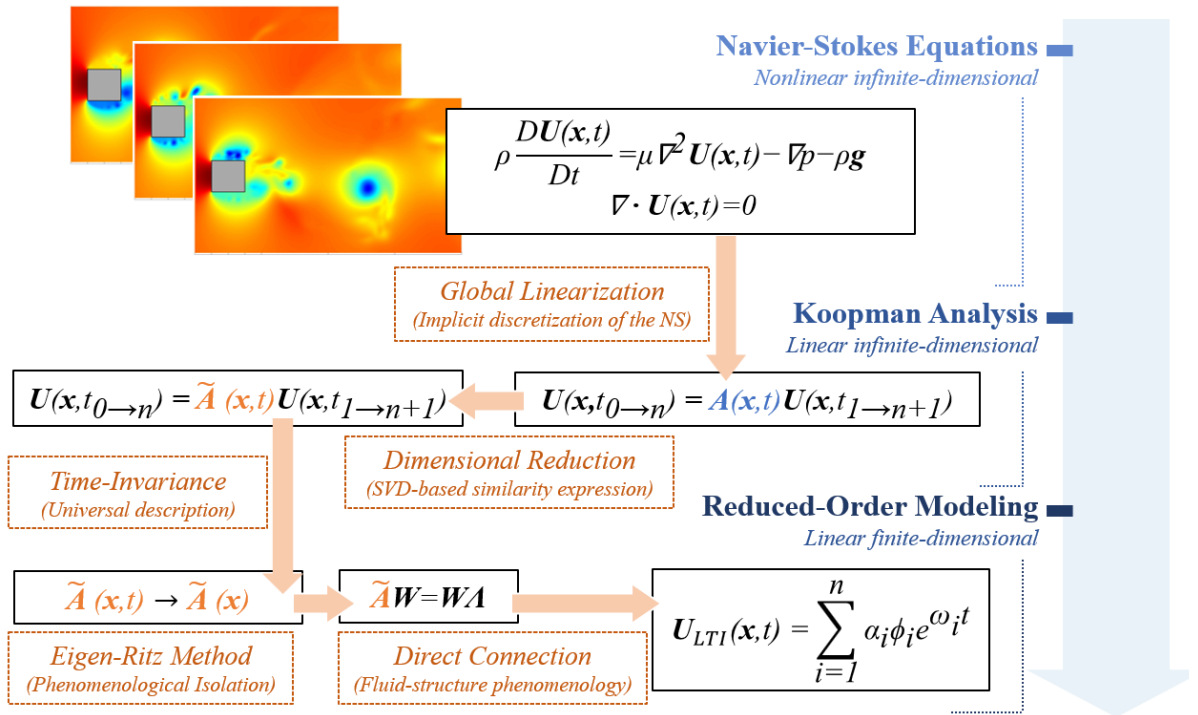


Fig. 1 A conceptual rundown of the Koopman Linearly Time-Invariant Decomposition (Koopman-LTI)

Sailing with the theoretical promise, this visionary prelude practically demonstrates and substantiates the possibility of the Koopman-LTI decomposition by successfully 1) constructing an accurate representation of a nonlinear, turbulence-rampant fluid-structure system, 2) decomposing the entwined morphologies from unprocessed data into isolated

constituents of distinct periodicities, and 3) establishing concrete and direct connections between the behaviors of the fluid and structure with phenomenological visualization.

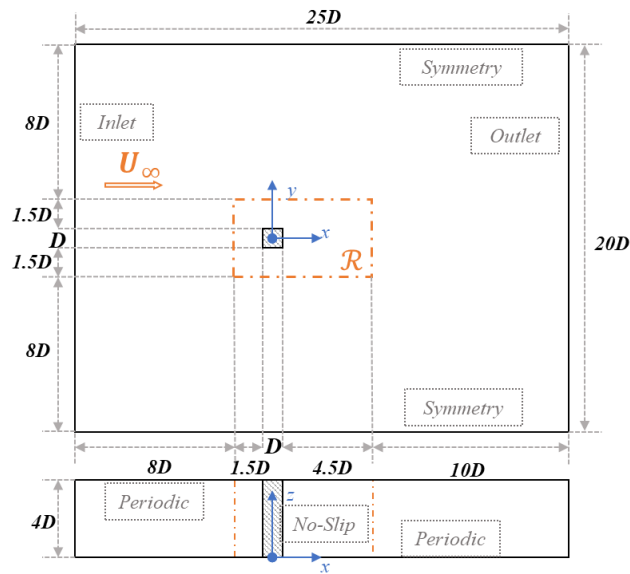
Numerical Details of Test Case

As the subject of study, we chose a prototypical configuration—subcritical free-shear flow past a stiff square prism—for the broadest applicability. This configuration is geometrically simplistic but phenomenologically complicated, involving stagnation, forced separation, reattachment, *etc.* [17], [18]. The four prism walls are also behaviorally complex and distinct [19], [20], and an infinite spanwise length prevents three-dimensional complications [21], [22]. In essence, we aim to present the most fundamental yet sufficiently sophisticated case to encourage empathy from the readership. We also deliberately selected the turbulent regime because success on random and anisotropic turbulence would tell a great deal about the technique’s generality and suitability, not only for systems in fluid mechanics, but also those in other disciplines. To this end, inlet perturbation is spared to avoid synthetic dynamics. In addition, we chose $Re=22,000$ because a shear layer undergoes the turbulence transition in this moderate subcritical regime, which appeals to phenomenological similitude for a wide range of Re [23]. This Re also permits high-fidelity simulation with an acceptable expense and has a plethora of literature for validation [18], [24], [25].

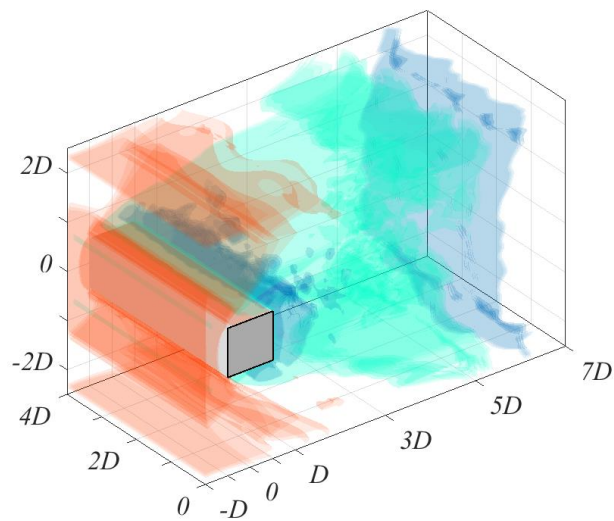
We decided to employ numerical data in this work because it is precise. Whilst error, hence inaccuracy, is possible for numerical data, noise contamination is unlikely. As the Koopman-LTI is highly sensitive to frequency content, prevention or elimination of noise is critical. Numerical data is also high-dimensional. In practice, data collection of any sort, regardless of field, experiment, or numerical, inevitably reduces the dimension of fluid systems from infinite to finite. Notwithstanding, the fine spatial discretization needed to resolve turbulence guarantees high-dimensionality, whereas field and experimental data are acutely limited by the measuring apparatus.

We employed the Large-Eddy Simulation with Near-Wall Resolution (LES-NWR) to simulate the turbulent flow [26]. The subgrid-scale motion is modeled by the Smagorinsky model [27] with the Lilly formulation [28], and the dynamic-stress model to obtain the Smagorinsky coefficient [29] [30]. **Fig. 2a** illustrates the computational domain and boundary conditions prescribed to the simulation. For validation, we present the LES_{IQ} proposed by Celik *et al.* [31] herein to succinctly demonstrate the quality of our LES-NWR. **Fig. 2b** presents the 92%, 93.5%, and 95% iso-surfaces of the LES_{IQ} . While LES-NWR requires only $>80\%$ resolution, our grid

achieves $>90\%$ everywhere. This resolution approaches a Direct Numerical Simulation (DNS) and attests to a proper LES-NWR. We refer readers to our previous work [32] for comprehensive numerical details and case validation.



a)



b)

Fig. 2 a) Computational domain and boundary conditions of the LES-NWR-simulated turbulent free-shear flow; b) Iso-surfaces of LES_{IQ} validating the LES-NWR grid: 92%-blue, 93.5%-mint green, 95%-orange

Results and Discussion

Time Invariance and Mechanism Isolation

Time invariance of the Koopman operator $\tilde{\mathcal{A}}(\mathbf{x}, t) \rightarrow \tilde{\mathcal{A}}(\mathbf{x})$ is a critical aspect of the technique, because it defines a consistent set of governing mechanisms. In practice, an indispensable prerequisite is to sample mean-subtracted data in the full statistical stationary state [32]. Moreover, the input sequences shall all reach the *Stabilization* state of DMD sampling, which guarantees the time-independence in data sampling [32], [33]. In this work, the five input data sequences for the Koopman-LTI correspond to the pressures of the four prism walls and the flow field. They are sampled and analyzed independently without any algorithmic communication. The vanilla DMD algorithm employed herein is also completely physics-uninformed.

In terms of results, we first examine the stability of the Koopman-LTI systems. **Fig. 3** displays the $\Re\text{-}\Im$ spectra, in which each Ritz pair corresponds to a pair of DMD conjugates or poles on the Z-space. Evidently, all poles lie very close to the $\Re^2 + \Im^2 = 1$ circle, exhibiting near-perfect oscillatory behaviors and stellar stability. Each pair also pertains to a unique frequency in continuous-time. We attribute the stability to the technique's exceptional ability to model periodic behaviors. Reminded of the Richardson-Kolmogorov's notion, turbulence is made up of eddies of different sizes, which translate precisely to motions of various periodicities in the wavenumber space [26]. Therefore, inputting fluctuating variables yields outstanding stability of the Koopman-LTI systems. Quantitatively, the maximum l_2 normalized reconstruction error of all five data sequences at all computational nodes is capped at 10^{-11} , which is basically a numerical zero.

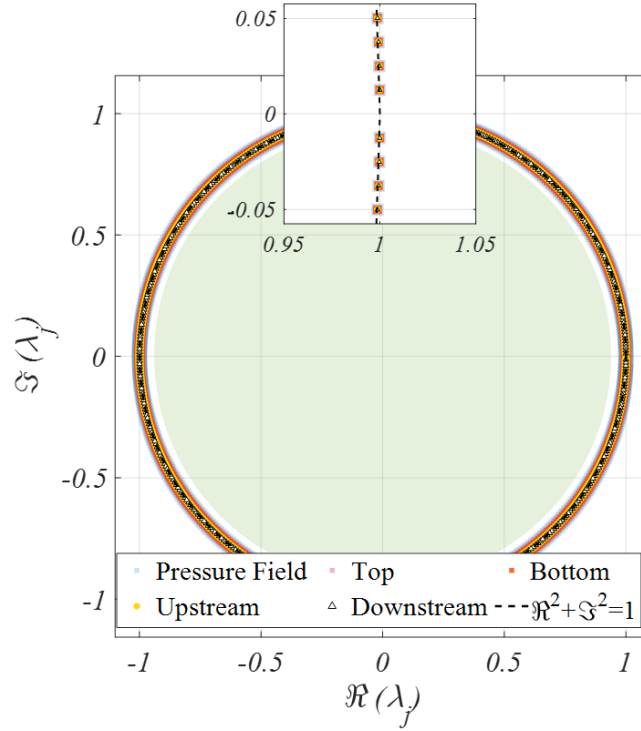


Fig 3. The \Re - \Im spectra (markers) and *Region of Convergence* (mint green) of the Koopman-LTI systems

Fig. 3 also illustrates the *Region of Convergence* (ROC) of the Koopman-LTI systems in mint green. The ROC contains the origin and is enclosed by poles and the $\Re^2 + \Im^2 = 1$ circle. These features characterize an anti-causal system, in which system behavior depends only on future inputs. This is concrete evidence of time-invariance. Furthermore, we note that all the poles of the five systems superpose perfectly onto one another, or equivalently speaking, they are identical. **This observation is of tremendous importance: despite the sampling and analytical autonomy of the five sequences, a case-wise overarching Koopman-LTI system exists and consists of the same frequency components, implying a universal set of underlying mechanisms.**

After close inspection of all modes, we confirm that the only difference between the five Koopman-LTI systems is the ranking of modal dominance by α_i (**Fig. 4**). To this end, the pressure field and pressures on the top (BC), down (AD), and upstream (AB) walls share similar behavioral trends, whereas the downstream (CD) wall exhibits smaller differences between the leading mode and the others. This echoes with the findings of Unal and Rockwell [34], as the pressure of the prism base is notably more sophisticated compared to those of the other walls. The modal amplitude also shows prominent peaks at specific frequencies analogous to the spectral density analysis. Should one envisage a bar-inscribing curve, its positive skewness

with a long tail to the right meets expectation, as the smaller, high-frequency eddies are less kinetically energetic but more in abundance.

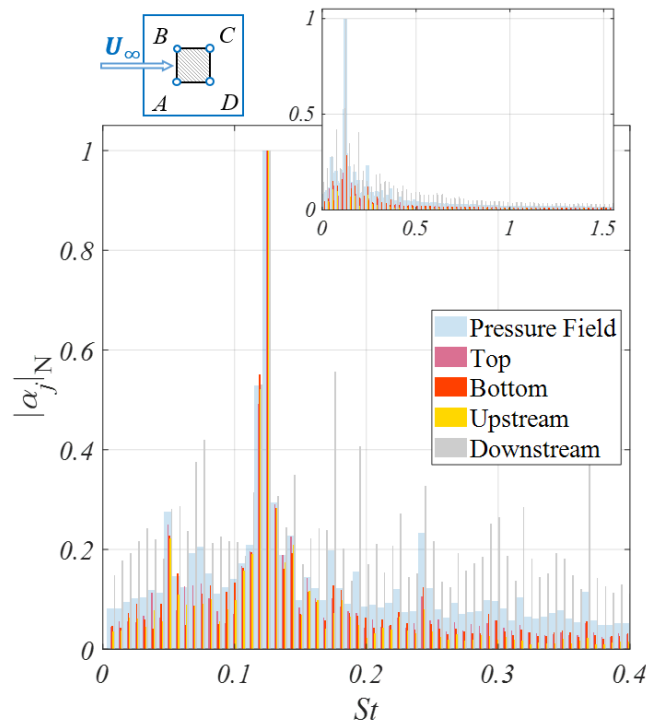


Fig. 4 Normalized leading coefficients α_j versus the Strouhal number, showing spatiotemporal dominance and distribution of modal frequency

Fig. 4 also illustrates how the **Koopman-LTI decomposes raw data that appears in an entwined morphology into isolated, distinct, and periodic constituents**. By mathematical formulation of the DMD, an input sequence containing N snapshots produces N independent constituents. We must clarify that the DMD-generated Ritz pairs differ from POD modes or principal component axes because they are not built on orthogonal bases. One may imagine performing a spectral analysis for the POD, after which the energy content of a POD mode basically distributes across several DMD modes. Moreover, since the turbulence spectrum is continuous, increasing N is equivalent to a refinement of spectral discretization. As $N \rightarrow \infty$, in principle $\tilde{\mathbf{A}}(\mathbf{x}, t) \rightarrow$ the Navier-Stokes Equations, and the discrete Z -transformation converges to the continuous Laplace-transformation $\mathcal{Z}(U[n]) \rightarrow \mathcal{L}(U(t))$.

Phenomenological Connections

The ensuing analysis is performed for the 20 most dominant modes. However, to preserve literary concision, we only present the mode shapes of Modes 1 and 4 in **Figs. 5** and **6**, respectively. Matching modal frequencies permit straightforward connections between the

phenomenology of the fluid and structure. Owing to the Ritz representation, one may also visualize the evolution of the mechanisms for every time instant ($t^* = \Delta t U_\infty / D$ reduced time) ([multimedia file](#)). Clearly, Mode 1 describes an alternatingly antisymmetric phenomenon that stems from flow separation, which triggers periodic bulging motions of the separation bubble before instigating synchronous shedding into the near-wake. The shed structures maintain the antisymmetry as they propagate, grow, and diminish further downstream. This field phenomenon is responsible for the periodic shift of positive and negative pressures on the cross-wind walls, and the axisymmetric alteration on the downstream wall. Given $St_1 = 0.124$ and its highest modal dominance, the mechanism described by Mode 1 is certainly a major component of the Bérnard-Kármán vortex shedding [35].

Mode 4 ($St_4 = 0.0497$) describes a very different scenario. This low-frequency activity begins at the trailing edge, and the near-wake exhibits less of a bulging motion but rather a vortex stretch. The shedding pattern is also unsynchronized and asymmetric, in which a dominant structure extends from the prism base along the central axis, and another weaker one forms towards either side. Interestingly, the dominant structure also maintains vortex sheets with its like-sign predecessor, until the weaker structure potentizes in strength and breaks the connection. Structure-wise, while the cross-wind walls are subjected to alternating pressures and clear reattachment, the prism base experiences an intense pressure gradient radiating from a central location. This information can be of great value. In a hypothetical engineering scenario, say for a building, to alleviate pressure extremities on the downstream façade, one shall certainly target and try to exterminate the field phenomenon described by Mode 4.

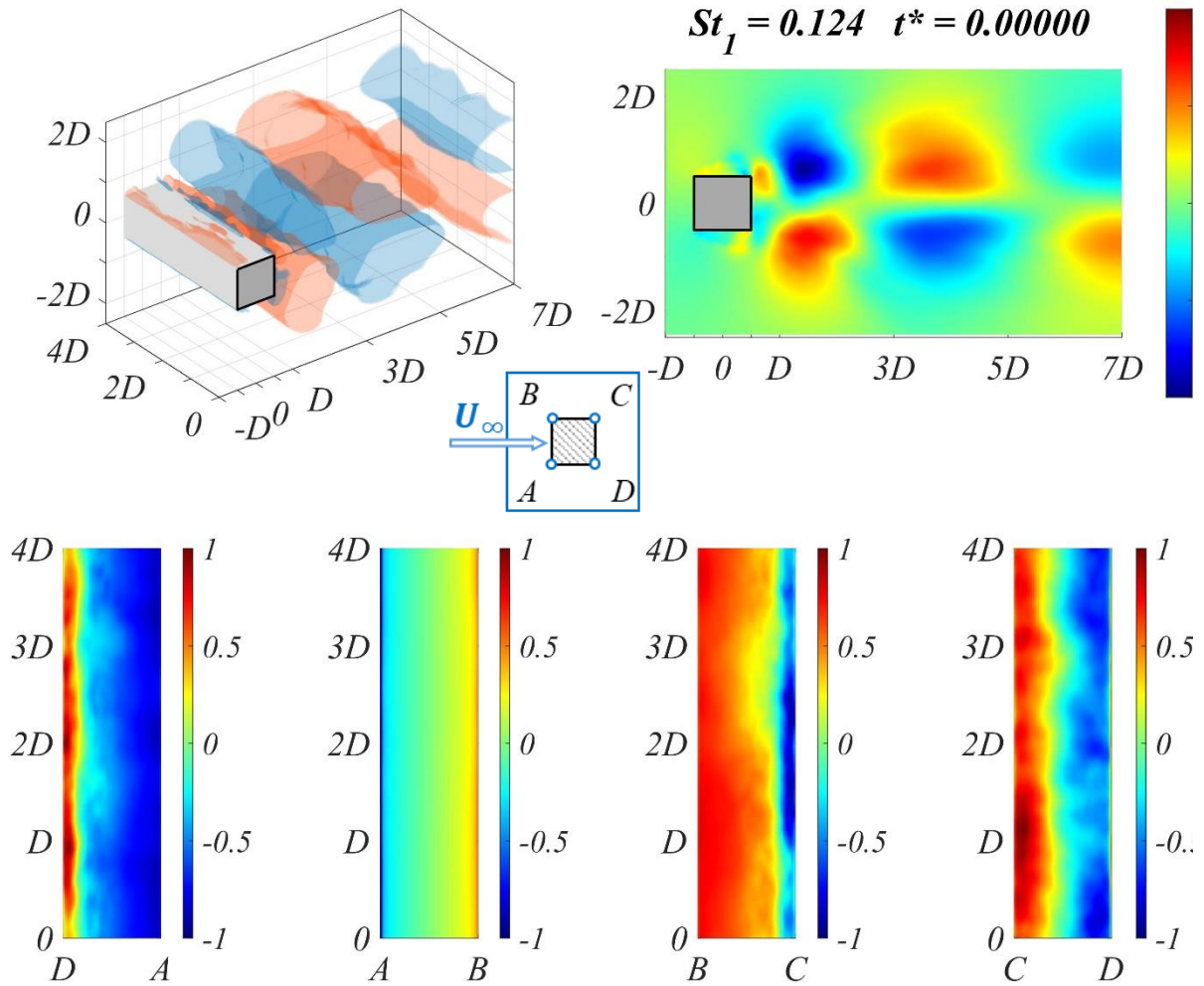


Fig. 5 Normalized mode shape (-1 to 1) of Mode 1 ($St_1 = 0.124$) at $t^*=0$ (generic). Top left: iso-surfaces ± 0.25 of pressure field. Top right: slice at mid-prism-span. Bottom from left to right: frequency matching mode shapes of the bottom, upstream, top, and downstream walls, respectively. ([Multimedia file](#) slowed by a factor of 500)

At this point, we elucidate the noteworthy implications of our work. **The Koopman-LTI decomposition permits direct connections of fluid and structure phenomenology, with which their independent and interactive behaviors are visualizable.** While the link can be somewhat established by other techniques, like spectral density or wavelet analysis, the visualization is generally unavailable. Other techniques like the Proper Orthogonal Decomposition (POD) grants orthogonal isolation and visualization, but without the frequency similitude, any attempt to associate the field and walls will rely heavily on user acumen, and even so, the speculations may be unwarranted. Therefore, the Koopman-inspired and DMD-implemented LTI system offers brand-new, physics-revealing insights into fluid-structure interaction. In terms of engineering application, one can now pinpoint the exact excitation mechanism(s) to target when trying to amplify or alleviate a specific structural behavior, or the

vice versa. The success with turbulence herein also testifies the technique's suitability for a broad array of complex fluid systems, if not many others beyond fluid mechanics.

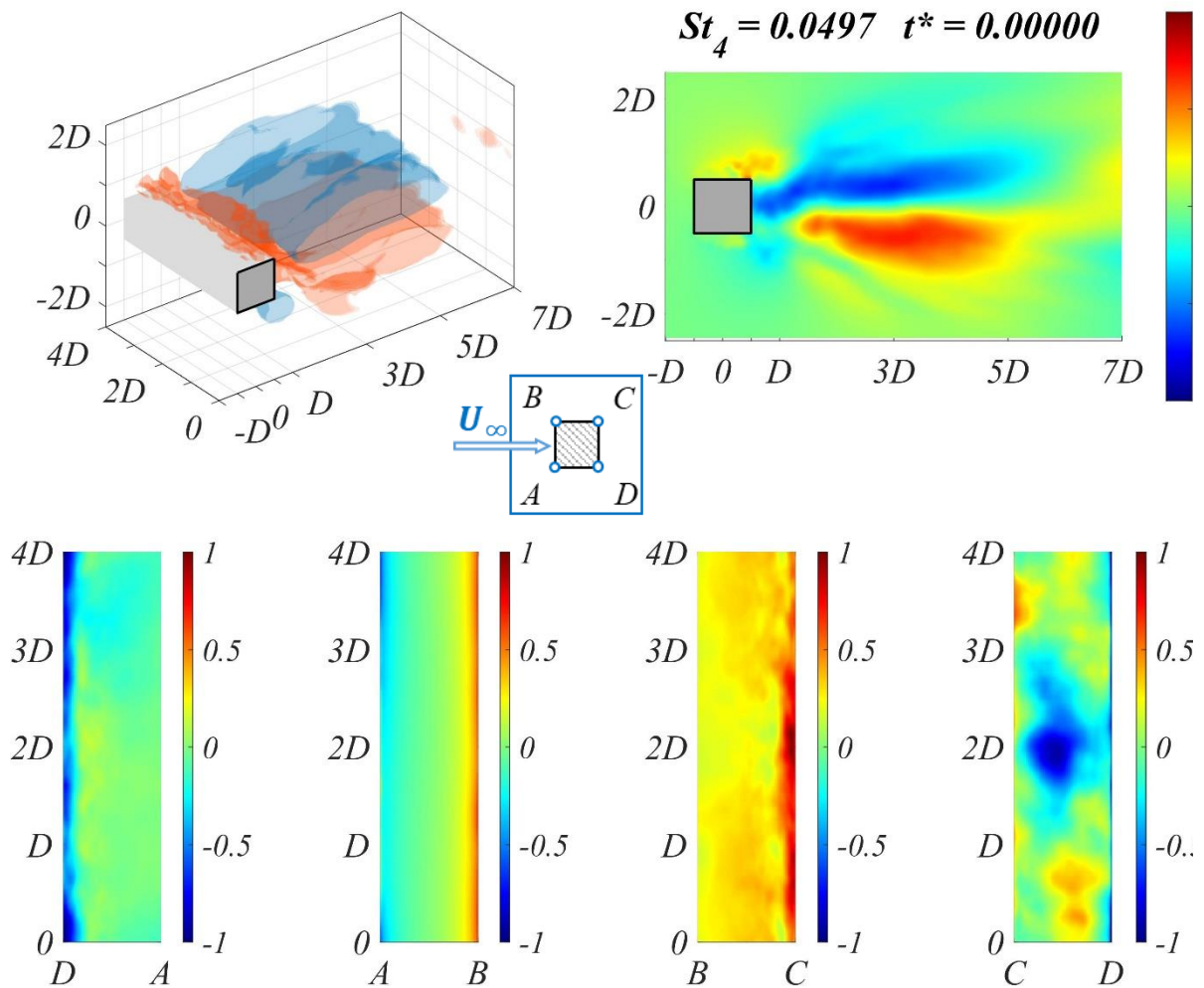


Fig. 6 Normalized mode shape (-1 to 1) of Mode 4 ($St_4 = 0.0497$) at $t^*=0$ (generic). Top left: iso-surfaces ± 0.25 of pressure field. Top right: contour sliced at mid-prism-span. Bottom from left to right: frequency matching mode shapes of the bottom, upstream, top, and downstream walls, respectively. ([Multimedia file](#) slowed by a factor of 500)

Now, we must outline some limitations, at least for the time being, of the technique. First, since each DMD mode represents a group of similar-size eddies moving at similar convective velocities, the number of DMD modes can essentially extend to infinity. Consequently, data management becomes a strenuous task. The MATLAB implementations of the current work expended up to 512 GB of RAM and 10 TB of storage, which can be demanding for ordinary computational platforms. Second, the criterion for dominance ranking is critical. Unlike the singular value for the POD, a spatiotemporal index must strike a proper balance in the weighting of energy and time. As we [33] and other researchers [15], [16], [36] have shown, certain low-energy states may have high dynamical relevance. To date, although several criteria

have been proposed [15], [37]–[40], there is yet a universal consensus. Third, errors will always ensue from the Koopman linearization. Although they are miniscule for this specific case, they may be significant for more sophisticated systems. Users shall always be mindful that any decomposition based on a lackluster LTI approximation is utterly inauspicious, if not adversely misleading. Finally, the current findings are based on a statistical stationary flow. Applicability to transient flows demands future investigation.

Conclusion

In this work, we demonstrated and corroborated a novel, data-driven, Koopman-inspired, and Dynamic Mode Decomposition-executed formulation called the Koopman Linearly Time-Invariant (Koopman-LTI) decomposition. Through an analysis of a subcritical turbulent free-shear flow, the results proved the Koopman-LTI capable of building a configuration-wise universal representation that approximates turbulence and FSI with stellar accuracy, where the maximum l_2 error is capped at 10^{-11} . Moreover, the Koopman-LTI decomposes the entwined morphologies of raw data into a linear superposition of distinct constituents. It also successfully established direct connections between fluid and structural behaviors by generating matching modes. With phenomenological visualizations, one may pinpoint exactly which fluid phenomena causes a specific structural response, or the vice versa.

Acknowledgements

We give a special thanks to the IT Office of the Department of Civil and Environmental Engineering at the Hong Kong University of Science and Technology. Its support for the installation, testing, and maintenance of our high-performance servers is indispensable for the current project. The work described in this paper was supported by a grant from the Research Grants Council of the Hong Kong Special Administrative Region, China (Project No. 16207719).

Funding

The work described in this paper was supported by the Research Grants Council of the Hong Kong Special Administrative Region, China (Project No. 16207719).

Conflict of Interest

The authors declare that they have no conflict of interest.

Availability of Data and Material

The datasets generated during and/or analyzed during the current work are restricted by provisions of the funding source but are available from the corresponding author on reasonable request.

Code Availability

The custom code used during and/or analyzed during the current work are restricted by provisions of the funding source.

Author Contributions

All authors contributed to the study conception and design. Funding, project management, and supervision were performed by Tim K.T. Tse and Zengshun Chen. Material preparation, data collection, and formal analysis were led by Cruz Y. Li and Zengshun Chen, and assisted by Asiri Umenga Weerasuriya, Xuelin Zhang, Yunfei Fu, and Xisheng Lin. The first draft of the manuscript was written by Cruz Y. Li and all authors commented on previous versions of the manuscript. All authors read, contributed, and approved the final manuscript.

Compliance with Ethical Standards

All procedures performed in this work were in accordance with the ethical standards of the institutional and/or national research committee and with the 1964 Helsinki declaration and its later amendments or comparable ethical standards.

Consent to Participate

Informed consent was obtained from all individual participants included in the study.

Consent for Publication

Publication consent was obtained from all individual participants included in the study.

Reference

- [1] G. Kemp, R. K. Jaiman, and B. C. Khoo, “A high-fidelity numerical study on the propulsive performance of pitching flexible plates,” *Phys. Fluids*, vol. 33, no. 5, p. 051901, May 2021, doi: 10.1063/5.0049217.
- [2] Y. Liu, B. Huang, H. Zhang, Q. Wu, and G. Wang, “Experimental investigation into fluid–structure interaction of cavitating flow,” *Phys. Fluids*, vol. 33, no. 9, p. 093307, Sep. 2021, doi: 10.1063/5.0064162.
- [3] X. Li, Z. Lyu, J. Kou, and W. Zhang, “Mode competition in galloping of a square cylinder at low Reynolds number,” *J. Fluid Mech.*, vol. 867, pp. 516–555, 2019, doi: 10.1017/jfm.2019.160.
- [4] M. Raissi, Z. Wang, M. S. Triantafyllou, and G. E. Karniadakis, “Deep learning of vortex-induced vibrations,” *J. Fluid Mech.*, vol. 861, pp. 119–137, 2019, doi: 10.1017/jfm.2018.872.
- [5] F. Ren, C. Wang, and H. Tang, “Active control of vortex-induced vibration of a circular cylinder using machine learning,” *Phys. Fluids*, vol. 31, no. 9, p. 093601, Sep. 2019, doi: 10.1063/1.5115258.
- [6] L. Liang, W. Mao, and W. Sun, “A feasibility study of deep learning for predicting hemodynamics of human thoracic aorta,” *J. Biomech.*, vol. 99, p. 109544, Jan. 2020, doi: 10.1016/J.JBIOMECH.2019.109544.
- [7] X. Guo *et al.*, “Predicting plaque vulnerability change using intravascular ultrasound + optical coherence tomography image-based fluid–structure interaction models and machine learning methods with patient follow-up data: a feasibility study,” *Biomed. Eng. OnLine 2021 201*, vol. 20, no. 1, pp. 1–18, Apr. 2021, doi: 10.1186/S12938-021-00868-6.
- [8] S. Li, S. Laima, and H. Li, “Data-driven modeling of vortex-induced vibration of a long-span suspension bridge using decision tree learning and support vector regression,” *J. Wind Eng. Ind. Aerodyn.*, vol. 172, pp. 196–211, Jan. 2018, doi: 10.1016/J.JWEIA.2017.10.022.
- [9] G. Hu and K. C. S. Kwok, “Predicting wind pressures around circular cylinders using machine learning techniques,” *J. Wind Eng. Ind. Aerodyn.*, vol. 198, p. 104099, Mar. 2020, doi: 10.1016/j.jweia.2020.104099.
- [10] C. Y. Li, T. K. T. Tse, and G. Hu, “Dynamic Mode Decomposition on pressure flow field analysis: Flow field reconstruction, accuracy, and practical significance,” *J. Wind Eng. Ind. Aerodyn.*, vol. 205, p. 104278, Oct. 2020, doi: 10.1016/j.jweia.2020.104278.
- [11] L. Zhou, K. T. Tse, G. Hu, and Y. Li, “Higher order dynamic mode decomposition of wind pressures on square buildings,” *J. Wind Eng. Ind. Aerodyn.*, vol. 211, no. June 2020, p. 104545, Apr. 2021, doi: 10.1016/j.jweia.2021.104545.
- [12] Y. Yuan, K. Zhou, W. Zhou, X. Wen, and Y. Liu, “Flow prediction using dynamic mode decomposition with time-delay embedding based on local measurement,” *Phys. Fluids*, vol. 33, no. 9, p. 095109, Sep. 2021, doi: 10.1063/5.0064867.
- [13] H. Ping *et al.*, “Dynamic mode decomposition based analysis of flow past a transversely oscillating cylinder,” *Phys. Fluids*, vol. 33, no. 3, p. 033604, Mar. 2021, doi: 10.1063/5.0042391.
- [14] J. H. Tu, C. W. Rowley, D. M. Luchtenburg, S. L. Brunton, and J. N. Kutz, “On dynamic mode decomposition: Theory and applications,” *J. Comput. Dyn.*, vol. 1, no. 2, pp. 391–421, 2014, doi: 10.3934/jcd.2014.1.391.

- [15] P. J. Schmid, “Dynamic mode decomposition of numerical and experimental data,” *J. Fluid Mech.*, vol. 656, pp. 5–28, Aug. 2010, doi: 10.1017/S0022112010001217.
- [16] Y. C. Li *et al.*, “A Parametric and Feasibility Study for Data Sampling of the Dynamic Mode Decomposition—Part I: Range, Resolution, and Universal Convergence States,” Oct. 2021, Accessed: Oct. 15, 2021. [Online]. Available: <https://arxiv.org/abs/2110.06573v1>.
- [17] M. P. Paidoussis, S. J. Price, E. de Langre, M. P. Paidoussis, S. J. Price, and E. de Langre, *Fluid-Structure Interactions: Cross-Flow-Induced Instabilities*. Cambridge: Cambridge University Press, 2010.
- [18] F. Alves Portela, G. Papadakis, and J. C. Vassilicos, “The turbulence cascade in the near wake of a square prism,” *J. Fluid Mech.*, vol. 825, pp. 315–352, 2017, doi: 10.1017/jfm.2017.390.
- [19] D. C. Lander, C. W. Letchford, M. Amitay, and G. A. Kopp, “Influence of the bluff body shear layers on the wake of a square prism in a turbulent flow,” *Phys. Rev. Fluids*, vol. 1, no. 4, p. 44406, 2016, doi: 10.1103/PhysRevFluids.1.044406.
- [20] Z. Chen, X. Fu, Y. Xu, C. Y. Li, B. Kim, and K. T. Tse, “A perspective on the aerodynamics and aeroelasticity of tapering: Partial reattachment,” *J. Wind Eng. Ind. Aerodyn.*, vol. 212, no. October 2020, p. 104590, May 2021, doi: 10.1016/j.jweia.2021.104590.
- [21] Z. Chen, K. T. T. Tse, K. C. S. C. S. Kwok, and A. Kareem, “Aerodynamic damping of inclined slender prisms,” *J. Wind Eng. Ind. Aerodyn.*, vol. 177, pp. 79–91, Jun. 2018, doi: 10.1016/j.jweia.2018.04.016.
- [22] P. K. Kundu, *Fluid mechanics*, 3rd ed.. Amsterdam: Amsterdam : Elsevier Academic Press, 2004.
- [23] H. Bai and M. M. Alam, “Dependence of square cylinder wake on Reynolds number,” *Phys. Fluids*, vol. 30, no. 1, 2018, doi: 10.1063/1.4996945.
- [24] F. X. Trias, A. Gorobets, and A. Oliva, “Turbulent flow around a square cylinder at Reynolds number 22,000: A DNS study,” *Comput. Fluids*, vol. 123, no. 22, pp. 87–98, 2015, doi: 10.1016/j.compfluid.2015.09.013.
- [25] Y. Cao, T. Tamura, and H. Kawai, “Spanwise resolution requirements for the simulation of high-Reynolds-number flows past a square cylinder,” *Comput. Fluids*, vol. 196, p. 104320, Jan. 2020, doi: 10.1016/j.compfluid.2019.104320.
- [26] S. B. Pope, *Turbulent Flows*. Cambridge University Press, 2000.
- [27] J. Smagorinsky, “General Circulation Experiments with the Primitive Equations,” *Mon. Weather Rev.*, vol. 91, no. 3, pp. 99–164, Mar. 1963, doi: 10.1175/1520-0493(1963)091<0099:gcewtp>2.3.co;2.
- [28] D. K. Lilly, “The Representation of Small-Scale Turbulence in Numerical Simulation Experiments,” in *Proc. IBM Scientific Computing Symp. on Environmental Sciences*, 1967, pp. 195–210, doi: 10.5065/D62R3PMM.
- [29] M. Germano, U. Piomelli, P. Moin, and W. H. Cabot, “A dynamic subgrid-scale eddy viscosity model,” *Phys. Fluids A*, vol. 3, no. 7, pp. 1760–1765, Jul. 1991, doi: 10.1063/1.857955.
- [30] D. K. Lilly, “A proposed modification of the Germano subgrid-scale closure method,” *Phys. Fluids A*, vol. 4, no. 3, pp. 633–635, Mar. 1992, doi: 10.1063/1.858280.
- [31] I. B. Celik, Z. N. Cehreli, and I. Yavuz, “Index of resolution quality for large eddy simulations,” *J. Fluids Eng. Trans. ASME*, vol. 127, no. 5, pp. 949–958, 2005, doi: 10.1115/1.1990201.
- [32] Y. C. Li *et al.*, “A Parametric and Feasibility Study for Data Sampling of the Dynamic Mode

- Decomposition—Part I: Range, Resolution, and Universal Convergence States,” *Nonlinear Dyn.*
- [33] Y. C. Li *et al.*, “A Parametric and Feasibility Study for Data Sampling of the Dynamic Mode Decomposition—Part II: Input Variable, Truncation, Interpolation, and Cross-Validation,” *Nonlinear Dyn.*
- [34] M. F. Unal and D. Rockwell, “On vortex formation from a cylinder. Part 1. The initial instability,” *J. Fluid Mech.*, vol. 190, pp. 491–512, May 1988, doi: 10.1017/S0022112088001429.
- [35] C. Y. Li, T. K. T. T. Tse, G. Hu, and L. Zhou, “Modal Isolation and Physics Revelation of a Subcritical Free-Shear Flow by the Dynamic Mode Decomposition,” p. Under Review, Oct. 2021, Accessed: Oct. 15, 2021. [Online]. Available: <https://arxiv.org/abs/2110.06570v1>.
- [36] B. R. Noack, S. Michael, A. Boye, M. Gerd, M. Marek, and C. Pierre, “A Finite-Time Thermodynamics of Unsteady Fluid Flows,” *Journal of Non-Equilibrium Thermodynamics*, vol. 33. p. 103, 2008, doi: 10.1515/JNETDY.2008.006.
- [37] M. R. Jovanović, P. J. Schmid, and J. W. Nichols, “Sparsity-promoting dynamic mode decomposition,” *Phys. Fluids*, vol. 26, no. 2, p. 24103, 2014, doi: 10.1063/1.4863670.
- [38] J. Kou and W. Zhang, “An improved criterion to select dominant modes from dynamic mode decomposition,” *Eur. J. Mech. B/Fluids*, vol. 62, pp. 109–129, 2017, doi: 10.1016/j.euromechflu.2016.11.015.
- [39] X. Luo and A. Kareem, “Dynamics of random pressure fields over bluff bodies: a dynamic mode decomposition perspective.” Mar. 2019, [Online]. Available: <https://arxiv.org/abs/1904.02245>.
- [40] T. Sayadi, P. J. Schmid, F. Richecoeur, and D. Durox, “Parametrized data-driven decomposition for bifurcation analysis, with application to thermo-acoustically unstable systems,” *Phys. Fluids*, vol. 27, no. 3, p. 37102, 2015, doi: 10.1063/1.4913868.